

# Molecular BioSystems

Accepted Manuscript



This is an *Accepted Manuscript*, which has been through the Royal Society of Chemistry peer review process and has been accepted for publication.

*Accepted Manuscripts* are published online shortly after acceptance, before technical editing, formatting and proof reading. Using this free service, authors can make their results available to the community, in citable form, before we publish the edited article. We will replace this *Accepted Manuscript* with the edited and formatted *Advance Article* as soon as it is available.

You can find more information about *Accepted Manuscripts* in the [Information for Authors](#).

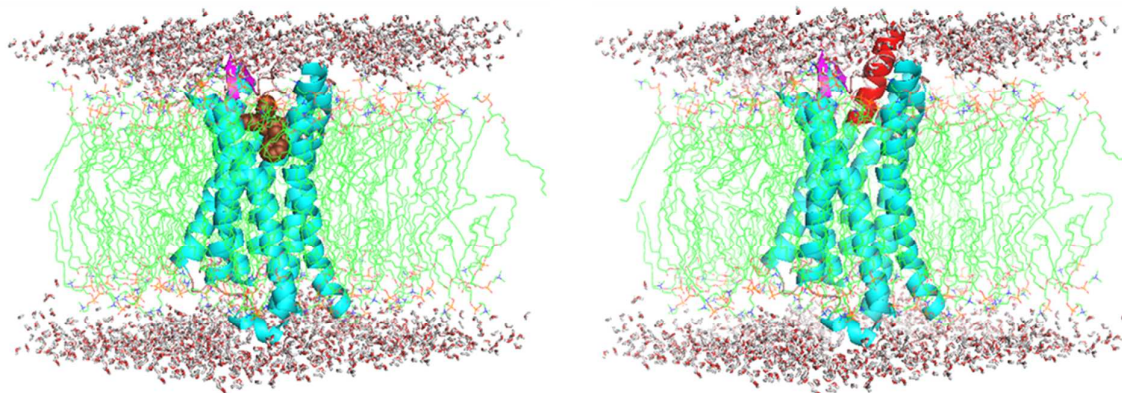
Please note that technical editing may introduce minor changes to the text and/or graphics, which may alter content. The journal's standard [Terms & Conditions](#) and the [Ethical guidelines](#) still apply. In no event shall the Royal Society of Chemistry be held responsible for any errors or omissions in this *Accepted Manuscript* or any consequences arising from the use of any information it contains.



[www.rsc.org/molecularbiosystems](http://www.rsc.org/molecularbiosystems)

**Graphical abstract for**  
**Nociceptin receptor (NOPR) and its interaction with clinically important agonist**  
**molecules: A membrane molecular dynamics simulation study**

Gugan Kothandan<sup>1\*</sup>, Changdev. G. Gadhe<sup>2</sup>, Anand Balupuri<sup>3</sup>, Jagadeesan Ganapathy<sup>5</sup>, Seung  
Joo Cho<sup>3,4\*</sup>



**Nociceptin receptor (NOPR) and its interaction with clinically important agonist  
molecules: A membrane molecular dynamics simulation study**

Gugan Kothandan<sup>1\*</sup>, Changdev. G. Gadhe<sup>2</sup>, Anand Balupuri<sup>3</sup>, Jagadeesan Ganapathy<sup>5</sup>, Seung Joo  
Cho<sup>3,4\*</sup>

<sup>1</sup>*Centre of Advanced Study in Crystallography and Biophysics, University of Madras, Guindy  
Campus, Chennai-600025, India*

<sup>2</sup>*Department of Life Science, College of BioNano Technology, Gachon University,  
San 65, Bokjeong-dong, Sujeong-gu, Seongnam-si, Gyeonggi-do 461-701, Korea*

<sup>3</sup>*Department of Bio-New Drug Development, College of Medicine, Chosun University, Gwangju  
501-759, Korea*

<sup>4</sup>*Department of Cellular · Molecular Medicine, College of Medicine, Chosun University,  
Gwangju 501-759, Korea*

<sup>5</sup>*Department of Physics, Presidency college, Chennai-600005, India*

\* Author for correspondence

E-mail: guganmsc@gmail.com, chosj@chosun.ac.kr

## Abstract

Nociceptin receptor (NOPR) is an orphan G protein-coupled receptor that contains seven transmembrane helices. NOPR has a distinct mechanism of activation, though it shares a significant homology with other opioid receptors. Previously there were reports on homology modeling of NOPR and further molecular dynamics simulation studies for a short period. Recently the crystal structure of NOPR has been reported. In this study, we analyzed the time dependent behavior of NOPR docked with clinically important agonist molecules such as NOP (natural agonist) peptide and compound 10 (SCH-221510 derivative) using molecular dynamics simulations (MDS) for 100 ns. Molecular dynamics simulation of NOPR-agonist complexes allowed us to refine the system and also to identify stable structures with better binding modes. Structure activity relationships (SAR) for SCH221510 derivatives were investigated and reasons for the activities of these derivatives were determined. Our molecular dynamics trajectory analysis of NOPR-peptide and NOPR-compound 10 complexes found residues crucial for binding. Mutagenesis studies on the residues identified from our analysis could be effective. Our results could also provide useful information for structure-based drug design of novel and potent agonists targeting NOPR.

Keywords: NOPR, SCH-221510, Molecular dynamics simulation, Docking

## Introduction

The Nociceptin receptor (NOPR) was identified and sequenced from the human and mouse genome in 1994 as an orphan GPCR.<sup>1</sup> It belongs to the family of G-protein coupled receptors and was initially called as opioid receptor-like receptor (ORL-1) because of its notable homology with classical opioid receptors. Since 2000, the name ORL-1 has been replaced as NOPR by the International Union of Basic and Clinical Pharmacology.<sup>2</sup> The NOPR's endogenous ligand, nociceptin/orphanin FQ (NOP) was discovered in 1995<sup>3,4</sup> and it has close resemblance with the kappa opioid receptor agonist (KOP) called dynorphin. The binding of NOP with the NOPR leads to the functional activation of NOPR, results in inhibition of cAMP synthesis and stimulation of  $K^+$  conductance, similar to the entire class of opiate receptors.<sup>5</sup>

NOPR is widely distributed throughout the brain and spinal cord. It is also present in peripheral nervous system and in some non-neural tissues and thus is expected to participate in a wide range of physiological events. Following the discovery of NOPR and its ligands, there has been remarkable advance toward understanding its pharmacological significance. The pathological and physiological roles of NOPR have been reviewed.<sup>6,7</sup> Both NOPR agonists as well as antagonists have a broad therapeutic potential. The agonists are used as antitussives, anxiolytics, vasodilators, hypotensives, and in the treatment of neuropathic pain, drug dependence, urinary incontinence, congestive heart failure, and anorexia.<sup>6</sup> However, antagonists are used as analgesics, antidepressants, nootropics, and in the treatment of obesity and Parkinson's disease.<sup>6</sup>

At present, only very few clinical trials have been done on NOPR selective ligands. The antagonist JTC-801 has been used in clinical trials for pain (Phases I and II, as reported in some

reviews, but clinical data are not available in the literature).<sup>6, 8</sup> A Phase I clinical trial has been proposed for the antagonist SB-612111 (GlaxoSmithKline) in the treatment of Parkinson's disease.<sup>6</sup> NOP has been used in clinical trials by intravesical administration in patients with overactive bladder<sup>9</sup> and the peptidic peripherally acting NOPR partial agonist ZP-120 (Zealand Pharma) has been used in a Phase II study as a diuretic in the treatment of acute heart failure.<sup>8</sup> There are, nevertheless, a lot of clinical data available for opioid drugs analogous to morphine which are also active on the NOPR. So it is of utmost interest to develop NOPR selective ligands, since NOPR is a potential drug target.

For any biological target the availability of an X-ray crystal structure can help in explaining the structure activity relationship (SAR) of reported compounds. One of the main reasons for the lack of selective ligand molecules (agonists and antagonists) targeting any biologically important receptor is because of the unavailability of X-ray crystal structure, especially in the case of GPCR's. The importance of three-dimensional structural information on protein drug targets can streamline many aspects of drug discovery, from target selection and target product profile determination, to the discovery of novel molecular scaffolds that form the basis of potential drugs, to lead optimization and its importance.<sup>10</sup> Moreover, three-dimensional structures have had a major impact on drug discovery, aiding the design of molecules with improved selectivity and pharmaceutical properties. With the availability of recently reported X-ray structure of NOPR (**PDB code: 4EA3**),<sup>11</sup> it is highly possible to develop novel selective ligands.

In this study, with the available X-ray structure of NOPR, combined *in silico* methodologies such as docking and molecular dynamics simulations studies were performed. We docked the natural agonist NOP, a small molecule agonist SCH-221510<sup>12</sup> and its derivative

(compound 10)<sup>13</sup> into the active site of the receptor. Molecular dynamics simulation was performed for 100 ns in the presence of membrane environment. The strategy employed here could be appropriate to understand the structure–activity relationship of NOP derivatives and deepens the knowledge of interaction mechanism between ligand and NOPR.

## Materials and methods

All molecular modeling calculations were performed using molecular modeling programs, Sybyl 8.1, AutoDock 4.0, GROMACS installed on a Linux environment.

### Modeling of NOP peptide

Nociceptin is a 17 amino acid peptide and the entire amino acid sequence was retrieved from the Uniprot database (accession number Q13519|130-146). Orsini and his coworkers have reported that this peptide was found to have a relatively stable helix conformation from residues 4–17.<sup>14</sup> The overall structure was considered to be an alpha helix and the structure of NOP was modeled using the biopolymer module in Sybyl.

### Structure preparation

The NOPR structure has been deposited recently in the protein data bank (PDB code: 4EA3).<sup>11</sup> The structure was then retrieved from the protein data bank and prepared for further study. The structure was a homodimer with a resolution of 3.01 Å and it could be possible to use any of the chains. We have selected A-chain in this study. The co-crystallized ligand molecule (peptide mimetic ONN) was first removed and the missing residues were built manually. All water molecules were removed and hydrogen atoms were added to the molecule using the Biopolymer structure preparation protocol within Sybyl 8.1.<sup>15</sup> The structure needs to be energy minimized in

order to remove bad contacts. Localized strain can be present due to small errors in the original structure such as bad Van der Waals contacts.

The models were refined by performing energy minimization in a vacuum assumption to relax from the strain. Steepest descent algorithm<sup>16</sup> and Gromos96 force field<sup>17</sup> was used for this refinement procedure and energy minimization was performed for 1000 steps. Similarly, the modeled NOP peptide was also refined by the above mentioned protocol. Moreover, the small molecule agonist SCH-221510<sup>12</sup> and its derivative (compound 10)<sup>13</sup> was also prepared. The geometries of these ligand molecules were optimized using the Tripos force field,<sup>17</sup> distance dependent dielectric constant and Powell's conjugate gradient methodologies.<sup>18</sup> Partial atomic charges were applied using the Gasteiger Huckel method.<sup>19</sup> The optimized ligand molecules with partial atomic charges were used in further docking study to predict the preferred orientation of the molecules inside the receptor active site and also to identify the key residues involved in contact with the ligand molecules.

### **Binding site and docking analysis**

Autodock 4.0 program was used for the docking calculations. Autodock uses the Lamarckian genetic algorithm (LGA) and is regarded as one of the reasonable docking program for most docking purpose.<sup>20</sup> Hydrogen atoms and the active torsions of ligand were assigned using Autodock tools (ADT). The binding site of NOPR was assigned based on the co-crystallized ligand molecule ONN and was extended (around 5 Å residues) up to 5 Å to guide the ligand molecule en route for possible orientation in the binding site. Autogrid was employed to generate grid maps around the active site using 60×60×60 points and a grid spacing of 0.375 Å. The docking parameters modified from defaults were; number of individuals in the population (set at

150), maximum number of energy evaluations (set at 2,500,000), maximum number of generations (set at 27,000), and number of GA runs (set at 100). The final structures were clustered and ranked according to the Autodock scoring function.

### **Protein -peptide docking**

The reported agonist (Nociceptin) consisting of 17 residues was docked against the receptor structure using the protein-protein docking server ClusPro 2.0.<sup>21</sup> ClusPro 2.0 has been reported as the best performing server in the latest rounds of CAPRI and we used it for our docking study. The procedure starts with the rigid body global search based on the Fast Fourier Transform (FFT) correlation approach that evaluates the energies of docked conformations on a grid. While ClusPro 1.0 used the docking programs DOT and ZDOCK, ClusPro 2.0 used a new program called PIPER. PIPER is also FFT-based, but the method is extended to be used with pair-wise interaction potentials. The number of structures is reduced by rigid body filters based on empirical potentials and electrostatics calculations. Because of the use of the more accurate pair-wise potential in PIPER it is enough to retain 1000 structures, without the filtering step. The retained structures are clustered using the pair-wise RMSD as the distance measure and a fixed or variable clustering radius. The structures in these clusters are refined by a novel medium range optimization method called SDU (Semi-Definite programming based Underestimation), developed to locate the global energy minima within the regions of the conformational space defined by the separate clusters. This procedure was used in the latest rounds of CAPRI with very good results.

### Setup of the system in bilayer environment

To study the time dependent behavior of protein-ligand (peptide/small molecule) complexes, molecular dynamic simulation was done using GROMACS simulation package<sup>22</sup> in an explicit phospholipid bilayer. Protein, ligand (peptide/small molecule), lipid and water molecules were used as components for the simulation. The GROMOS96 force field<sup>22</sup> was used and the lipid bilayer was developed using specific topology files, as described by Tieleman<sup>23</sup> (<http://moose.bio.ucalgary.ca>), was used in the present study.

To obtain a better starting structure, we used the InflateGRO script from Prof. Tieleman website (<http://moose.bio.ucalgary.ca>) to pack lipids around an embedded protein. The starting point with this method is a pre-equilibrated bilayer into which the protein ligand (peptide/small molecule) complex has already been “inserted” in the lipid bilayer but fully overlaps with lipids. The system cannot be energy minimized due to extreme overlap. The bilayer was expanded using a scaling factor of 4 and a distance cut-off of 14 Å. Overlapping lipid molecules was deleted. For estimating the area per lipid a grid size of 5 Å was used. Energy minimization was done using strong position restraints to ensure that the structures don't change at all. Energy minimization was then followed by compression using a scaling factor of 0.95. Compression and energy minimization steps were repeated until the area per lipid converges to the reference value (0.62-0.64) for the lipid species used.

The system was then solvated with TIP3P water box<sup>24</sup> by increasing the van der Waals radius of carbon atoms from 0.15 to 0.5, so to prevent water molecules from being placed in the hydrophobic section of the bilayer.<sup>25</sup> Once the system got solvated, the van der Waals radius of C was again set to 0.15 Å. The system was further neutralized by adding appropriate counter ions

with a concentration of 0.15 M. Periodic boundary conditions were applied; the ligand topologies as well as the parameters were obtained from PRODRG server.<sup>26</sup> The parameterization methodology implemented in the PRODRG program is widely used in MD simulations of drugs; however, the applicability of PRODRG charges for molecular simulations has been questioned in the literature, because PRODRG doesn't reproduce topologies in the force field due to inconsistent charges and charge groups.<sup>27</sup> The partial charges are crucial in particular for a reasonably accurate description of non covalent interactions due to the long-range nature of electrostatic interactions and PRODRG underestimates charges for some atom types. To overcome this issue, we cross checked the topologies and we manually assigned charges.

After energy minimization, the system was subjected to a short NVT equilibration phase and it is further followed by a longer NPT phase. Generally a short NVT equilibration phase is followed by a longer NPT phase. The reason is that we are now dealing with a heterogeneous system [water and DPPC] as solvents. Such heterogeneity requires a longer equilibration process. Water has to reorient around the lipid head groups and any exposed parts of the protein, and the lipids have to orient themselves around the macromolecule. During equilibration, the macromolecule (protein-ligand) was position restrained so that it allows the solvents to equilibrate around our protein structure without any structural changes in the protein. NVT ensemble was done at constant temperature of 310 K for a period of 100 ps and then followed by NPT ensemble for a period of 1 ns. Modified Berendsen coupling scheme was employed in both the ensembles, particle mesh Ewald (PME)<sup>28</sup> method was used to calculate long-range electrostatics. Parinello and Rahman coupling scheme was used as barostat for pressure coupling and semi-isotropic pressure coupling was applied with reference pressure (1.0 bar), which is intended for membrane simulations. All bond lengths were constrained using the LINCS

algorithm<sup>29</sup> and SETTLE algorithm was used to constrain the geometry of water molecules.<sup>30</sup> Final production run was performed for a period of 100 ns.

## Results

### Modeling of NOP peptide and structure preparation of NOPR

Nociceptin is a 17 amino acid peptide and was reported to be having stable alpha helical conformation for residues 4-17.<sup>14</sup> Keeping this in mind, the overall structure was considered to be an alpha helix and the three dimensional structure of NOP peptide was modeled. The modeled structure of NOP peptide and the already available NOPR (PDB code: 4EA3) was then prepared for docking simulations. The modeled NOP peptide and the NOPR structures were further prepared by the biopolymer structure preparation tool in Sybyl. The prepared structures were then refined by simple energy minimization in vacuum using Gromos96 force field. The energy minimized NOP peptide and NOPR structures using molecular dynamics simulation (MDS) are shown in **Fig. 1a** and **Fig. 1b**.

### Binding site construction of NOPR

The NOPR structure highlights specific residues in the binding pocket that are essential for binding and to address the receptor subtype selectivity. The binding pocket of NOPR is relatively large, reflecting its ability to bind large peptide structures. The crystal structure of NOPR with the co-crystallized ligand molecule ONN allowed us to determine the affinity of new molecules targeting NOPR. The binding site was assigned based on the co-crystallized ligand molecule (ONN) and was extended around 5 Å residues. The binding site is composed of residues such as Tyr58, Thr103, Gln107, Asp110, Ile111, Val126, Ile127, Asp130, Tyr131, Met134, Phe135, Cys200, Leu201, Val202, Ile219, Phe220, Trp276, Val279, Gln280, Arg302 and Tyr309. The

residues composed from the binding pocket to guide docking are shown in **Supplementary Fig. S1**.

### **Molecular docking of SCH221510 and its derivative**

As the binding pocket projected here is the available crystal structure, one of the potent NOPR agonist, SCH-221510 ( $K_i = 0.3$  nM,  $p K_i = 9.52$ ) was docked into the binding site. 100 conformations were generated and the top ranking conformational clusters from our docking study were evaluated. The conformations within the top ranked cluster were then selected for analysis. It is well known that the top scoring binding mode is not always the correct binding mode in docking runs, even when ligands were docked into their own x-ray crystal structure. In cross docking experiments the top binding mode is rarely the native binding conformation. So, we carefully analyzed the conformations within the top cluster and a conformation was selected based on scoring function, interaction with crucial amino acid residue (Asp130) and other residues in the binding site.

At first we analyzed the docking results of SCH-221510. It was observed that the top cluster consists of 52 conformations within the cluster. The molecule SCH-221510 bound with a binding energy of -8.11 kcal / mol and an intermolecular energy of -9.6 kcal / mol. In addition, the ligand established crucial interactions with important residues in the binding site. The protonated nitrogen atom in the tropane ring formed a hydrogen bonding interaction with crucial and conserved Asp130, and the distance between the glutamic acid residue and the nitrogen atom was found to be 1.9 Å. Moreover the phenyl ring attached to the tropane ring resides in the hydrophobic pocket lined by Tyr131, Tyr132, Met134, Phe135 and Ile219. Furthermore, it was observed that the two phenyl rings attached to the carbon atom next to the nitrogen atom of the tropane ring faced the opposite side of receptor structure. These hydrophobic phenyl rings

oriented towards hydrophobic residues such as Val126, Ile127, Leu201 and Val202. In addition to the hydrogen bonding and hydrophobic contacts, we found that residues, such as, Gln107, Ser223, Gln280, Tyr309 are in the vicinity of ligand (within 4 Å). The docked orientation of the ligand molecule and its interaction with active site residues is shown in **Fig. 2**.

A series of highly active and selective NOPR agonists have been reported in the literature.<sup>13</sup> One of the potent derivatives of this series, compound 10 ( $K_i = 5$  nM,  $pK_i = 8.30$ ) was also docked into the binding site. It was found that the top cluster consists of 75 conformations within the cluster. The molecule bound with a binding energy of -7.84 kcal / mol and an intermolecular energy of -9.34 kcal / mol. As this derivative is similar to that of SCH-221510, the ligand observed similar orientation as that of SCH-221510. Similarly, the nitrogen in the tropane ring hydrogen bonded with crucial and conserved Asp130. In addition the nitrogen atom in the pyridine ring found to interact with Gln280. This ligand also established similar orientation with the active site residues as that of SCH-221510. The binding orientation of compound 10 is shown in **Fig. 3**.

### **Molecular docking of NOP peptide**

ClusPro 2.0 was used to dock the NOP peptide against NOPR. Previously the binding of NOP peptide to NOPR have been modeled and already reported in the literature. Topham *et al.*, and Akuzawa *et al.*, have used the inactive state of NOPR and proposed the binding of NOP peptide.<sup>31, 32</sup> More recently binding of NOP peptide to an active state NOPR was modeled and reported in the literature.<sup>33</sup> As the x-ray crystal structure of NOPR have been recently reported,<sup>11</sup> the binding of NOP peptide was modeled by performing protein-protein docking studies to obtain the most likely binding mode between NOPR and NOP peptide.

Docked models were generated with different forces of interaction between them. Previously it has been proposed that Asp130 is involved in a salt bridge interaction with positively charged N-terminal region (FGGF - message domain) of NOP peptide.<sup>31,32</sup> Since we have the knowledge that electrostatic interaction between crucial residues (Asp130-N-terminal of peptide) dominates the interaction, we analyzed the electrostatically favored coefficients. Four clusters have been reported in the electrostatically favored coefficients and each cluster contains lot of members in it. Each cluster has been analyzed and a cluster was selected based on interaction between Asp130 of NOPR and the N-terminal (FGGF) of peptide which is considered to be crucial. The selected cluster composed of 41 conformers within the cluster with the lowest energy score of -1450.6.

Our docking results identified that NOP peptide had crucial interactions with the receptor. The crucial N-terminal region of the peptide lies deep inside the pocket. It was observed that Phe1 of peptide, hydrogen bonded with crucial Tyr309 of receptor.<sup>11</sup> N-terminal residues Gly2 (N-H) and Gly3 (N-H) were found to be interacting with O2 of Asp130. These interactions indicate the importance of Asp130 which is in line with previous results.<sup>31,32</sup> Moreover, Phe4 (N-H) of the message domain found to be interacting with Tyr131. In addition, Lys9 hydrogen bonded with Asp110 and Glu199. It was also observed that the C-terminal residue, Lys13 hydrogen bonded with Gln192, Glu197 and Glu199 respectively. Moreover, Arg12 and Gln17 interacted with Asp195 of the receptor. In addition to these hydrogen bonding interactions, hydrophobic interactions were also observed between the peptide and the receptor. The docked mode of the agonist (NOP) with NOPR is shown in **Fig. 4**.

### Molecular dynamics simulation of receptor-agonist-membrane complexes

As NOPR is a membrane protein, an appropriate representation of NOPR should be embedded in a membrane environment with water molecules. *In vivo* binding of ligand to a receptor structure is a dynamic process. So to mimic the real biological environment, molecular dynamics simulation of NOPR-agonist complexes embedded in a lipid layer was done. Accordingly, we have analyzed the MD simulation of the docked model of NOPR-NOP peptide and NOPR-SCH derivative (compound 10). The strategy employed in this study could help us to identify the most stable and low energy conformation of receptor ligand complexes. The selected conformation of agonists (NOP and compound 10) inside the receptor could be assumed as the bioactive one. Since other derivatives in the dataset have similar core structure and variations in only substitutions, the selected stable conformation of ligand-receptor complexes will allow us to understand the structure activity relationship studies of SCH221510 derivatives. Moreover, the model obtained and relaxed in the membrane environment could be more appropriate for the structure based design of novel NOPR agonists.

The selected docked conformations of NOPR-NOP peptide and NOPR-compound 10 of SCH complexed with NOPR were implanted in a rectangular box composed of a DPPC bilayer solvated with water molecules. Overlapping lipid molecules were deleted. It has been observed that, five lipid molecules were deleted in both the complexes using InflateGRO. After the deletion of overlapping lipids, the protein-agonists-lipid complexes were then shrunk until it reaches an area per lipid of  $0.65 \text{ \AA}^2$ , which is closest to the reference value for DPPC lipids. The protein-agonist-lipid complexes were then solvated by adding water molecules and appropriate counter ions [NOPR-compound 10; 34  $\text{Na}^+$  and 41  $\text{Cl}^-$ ; NOPR-NOP peptide: 34  $\text{Na}^+$  and 44  $\text{Cl}^-$ ] were added to neutralize the system. To overcome the structural artifacts, the system was then

energy minimized. The two systems (NOPR-compound 10 and NOPR-NOP peptide) composed of protein, agonist, lipids, water molecules and ions was then equilibrated and a final production run of 100 ns was performed. The tightly packed system (NOPR-compound 10-lipids-water molecules and NOPR-NOP peptide-lipids-water molecules) included in the production run is shown in **Fig. 5a** and **Fig. 5b**.

### **Structural analysis of NOPR-NOP peptide and NOPR-compound 10 complexes throughout production run**

A number of parameters needed to be examined to substantiate the physical stability of the receptor structure. The stability of the system was examined structurally as well as energetically during the course of simulation as a function of time. The total energy and root-mean square deviations of protein structure versus initial structure were used as parameters to monitor the stability of the system.

At first, we analyzed the NOPR-NOP peptide complex. The total energy plot of the system indicated that the total energy decreased gradually until 4 ns and then stabilized at this level. Trajectory based analysis revealed the total energy of the system decreased from  $-2.39 \times 10^5$  KJ / mol to  $-2.45 \times 10^5$  KJ / mol. It was observed that most of the structures are around  $-2.43 \times 10^5$  KJ / mol, indicating that the systems were energetically stable. The NOPR structure was also evaluated on the basis of structural stability using RMSD calculated by structural variations with respect to time; the initial period was considered as period of equilibration. There was a gradual increase in RMSD to 0.42 till 42 ns. This was then followed by a plateau, which for most of the structures occurred at around  $0.42 (\pm 0.02)$  nm till 100 ns. These results indicated the structural stability of the model and stressed the importance of long run. The RMSD of peptide (NOP)

molecule and the movement of the ligand atoms throughout the simulation were also analyzed. It was observed that the initial conformation gradually moved to 0.33 nm till 4 ns, and then gradually decreased to 0.30 ( $\pm 0.02$ ) ns around 5 ns. This was then maintained throughout the simulation till it reaches 90 ns. A slight increase in RMSD (0.4 nm) was found and it fall back to 0.3 nm ( $\pm 0.02$ ). These results suggest that this ligand is stable throughout the simulation. The total energy plot and the RMSD plot of the receptor and ligand molecules are shown in **Fig. 6a** and **Fig. 6b**, respectively.

Similarly, the stability of NOPR-compound 10 complex was analyzed structurally and energetically. It was observed that the total energy of the system decreased from  $-2.36e+05$  KJ / mol to  $-2.42e+05$  KJ / mol and the average low energy structures are around  $-2.39e+05$  KJ / mol, indicating the system was energetically stable. The structural stability of the model was also analyzed by calculating the RMSD with respect to time. There was a gradual increase in RMSD to 0.3 nm till it reaches 40 ns. It was then maintained the same level ( $\pm 0.02$  nm) throughout the simulation till it reaches 100 ns. We then analyzed the movement of ligand molecule throughout the simulation with respect to time. The ligand molecule raised to 0.1 nm around 3 ns and it was maintained throughout the simulation with fluctuations of  $\pm 0.03$  nm over the course of time. The total energy plot and the RMSD plot of the receptor and ligand molecules are shown in **Fig. 6c** and **Fig. 6d**, respectively.

### **Binding mode and trajectory analysis (NOPR-compound 10)**

We first analyzed the trajectories and binding mode of SCH221510 derivative (compound 10). It was observed from the structural analysis; the ligand molecule (compound 10) was moved from initial position inside the proposed binding site (**Fig. 6d**). This stressed the importance and

practical relevance of molecular dynamics simulation after initial rigid docking analysis. The selected docked mode after initial rigid docking observed that, the protonated nitrogen in the tropane ring formed a hydrogen bonding interaction with crucial and conserved Asp130. As the interaction is crucial we monitored the hydrogen bonding pattern between them throughout the simulation. Our results show the importance of this interaction for activity and complement previous results [11]. We monitored the distance between the Asp130 and the nitrogen atom of tropane ring (**Fig. 7a**). The hydrogen bonding between Asp130 and protonated nitrogen of tropane ring throughout the simulation is also plotted and is shown in **Fig. 7b**. Our results stressed the importance of this residue.

Our initial rigid docking of compound 10 observed hydrophobic interactions with Tyr131, Tyr132, Met134, Phe135 and Ile219. We examined the time-dependent fluctuation of the distances between these residues and ligand molecule throughout the simulation. We observed that the residues (Tyr131 and Met134) stayed in vicinity throughout the simulation, whereas residues such as Tyr132 and Phe135 were not in vicinity after the period of equilibration (**Fig. 8a** and **Fig. 8b**). This implies the importance of Tyr131 and Met134 which is in agreement with previous mutational studies.<sup>11</sup> We also monitored the movement of Ile219 and Ser223 (**Supplementary Fig. S2a**) and we found that the residue (Ile219) could be crucial as this residue stayed in vicinity most of the time.

Furthermore, it was observed that the ligand molecule oriented towards hydrophobic residues such as Val126, Ile127, Leu201 and Val202 (**Fig. 3**) from our rigid docking analyses. We monitored the importance of these residues and we found that these residues are not in vicinity. Residues such as Val126 and Ile127 (**Supplementary Fig. S2b**) were around 0.5-0.6 nm, whereas Leu201 and Val202 moved out of vicinity completely as it was around 1 nm. We also

monitored residues such as Gln107, Ser223, Trp276, Gln280, Tyr309 through our trajectory analyses and we observed that Gln107 and Tyr309 are crucial and in agreement with previous mutational studies. However, we found that Ser223 may not be crucial (**Supplementary Fig. S2a**) and the residues Trp276 and Gln280 might be crucial and mutational studies could be effective. Time evolution of the distances between these residues and the ligand molecule during the simulation is displayed in **Supplementary Fig. S3**. The binding mode of compound 10 in the binding pocket after MDS leads to introduction of some new residues such as Asp97, Val100, Gly308 and Ser312 into the binding pocket compared with docking. The binding mode of compound 10 inside the binding site after MDS is shown in **Supplementary Fig. S4**.

#### **Binding mode and trajectory analysis (NOPR-NOP peptide)**

We then analyzed the trajectories and binding mode of NOP peptide similar to that of compound 10. It was observed from the structural analysis, the peptide agonist moved from its initial position inside the binding site (**Fig. 6b**). Our initial docking analysis identified that Phe1 hydrogen bonded with crucial Tyr309, Gly2 and Gly3 were found to be interacting with Asp130 and Phe4 hydrogen bonded with Tyr131. But in the case of NOPR-NOP peptide complex after MDS, we found that Phe1 hydrogen bonded with Tyr309 and in addition it also formed a hydrogen bond interaction with Gln107 which complements previous mutational results.<sup>11</sup> In addition, Gly2, Gly3 and Phe4 hydrogen bonded with Asp130. However, there is a shift in hydrogen bonding interaction with Tyr131 from Phe4 of peptide to Gly3 of peptide. These results stressed the importance of the message domain from NOP peptide and its interactions with crucial residues (Gln107, Asp130, Tyr131 and Tyr309) of the receptor. We monitored the fluctuation of the distances between these crucial residues and NOP peptide with respect to simulation time (**Supplementary Fig. S5**). Our results showed that residues such as Gln107,

Asp130 and Tyr309 stayed in vicinity throughout the simulation, whereas Tyr131 moved out for a period and then came back in vicinity. Our results stressed the importance of these residues and concur with previous mutational studies.<sup>11</sup>

We also observed the importance of residues such as Val126, Ile127, Met134, Ile219, Ser223, Trp276 and Gln280 which are in close proximity with that of message domain (FGGF) after MDS. Val126 and Ile127 stayed in vicinity throughout the simulation; however Met134 which was initially not in vicinity came back in vicinity after 20 ns. As mutagenesis studies on Met134 have already been done<sup>11</sup> and mutational studies on Val126 and Ile127 could be effective. The minimum distance between these residues and the peptide is shown in **Supplementary Fig. S6**. The analysis of the time-dependent fluctuation of the distances between NOP peptide and Ile219, Ser223, Trp276 and Gln280 residues showed that these residues were in close contact with peptide during the simulation (**Supplementary Fig. S7**).

Our rigid docking analysis identified that Lys9 hydrogen bonded with Asp110 and Glu199 and Lys13 hydrogen bonded with Gln192, Glu197 and Glu199 respectively. Whereas with the NOPR-NOP peptide complex obtained after MDS, we observed that there was an additional hydrogen bond between Arg8 of peptide and Gln286 of receptor. Lys9 (peptide) hydrogen bonded with Thr109 and Glu199. The hydrogen bond between Lys9 and Asp110 got vanished and instead it produced a hydrogen bond with Thr109. Though the C-terminal residues are not of importance we observed the interaction pattern between them and NOPR before and after MDS. There was a lot of difference in hydrogen bonding pattern between NOPR and peptide obtained after MDS. Arg12 and Gln17 interacted with Asp195 of the receptor, but in the case of NOPR-NOP peptide complex after MDS we observed that Arg12 and Gln17

hydrogen bonded with Gln291 and Asp209 respectively. The docked mode of the agonist (NOP) with NOPR after MDS is shown in (**Supplementary Fig. S8**).

### **SAR studies of SCH221510 derivatives from the perspectives of binding site after MDS**

The low energy conformation (NOPR-compound 10) obtained after MD simulations was further used to exploit the SAR's of SCH221510 derivatives. The binding mode of compound 10 ( $K_i = 5$  nM,  $pK_i = 8.30$ ) resulted from MDS was considered as a bioactive conformer (**Supplementary Fig. S4**). As compound 10 is the highly active molecule for a series of derivatives (**Table 1-3**) reported by Yang *et al.*,<sup>13</sup> we considered compound 10 as the representative molecule. We then compared the binding mode of this compound with those of the other molecules, since other molecules in the dataset are similar with varied substitution and SARs were explored.

Our trajectory analysis and the binding mode of compound 10 indicates that the hydrogen bonding between Asp130 and the protonated nitrogen atom of the tropane ring is crucial and it is necessary of potent activity. It was evident that hydrophobic substitution attached to the carbon atom of the tropane ring is necessary. This stressed the importance of basic nitrogen and the hydrophobic substitution for potent activity. This explains the greater activities of compounds such as compound 9, compound 11, compound 29, compound 30 and compound 32. Smaller substitutions such as fluoro, bromo, methyl, hydroxyl, or methylthio group (compounds 18-22) at the 5 position of the pyridine ring led to loss of activity. Substitution at this position is sterically restricted as it collides with Tyr131 of the receptor. This led to loss in activity compared to that of compound 10. Compound 9 which have 3-piperidynylmethyl substitution at the third position showed potent activity. The reason could be because of the room available to interact with Gln280 of NOPR (**Supplementary Fig. S4**). Compounds, 23 and 24 which has optimal

substitution at the same 3<sup>rd</sup> position lacks in activity. It implies that bulky substitution is needed at this position. Compounds (26-28) which has substitution at the 6<sup>th</sup> position are active; however they are less potent than that of compound 10.

We then focused on SAR of C-3-2-piperidinyll analogues such as compound 11-15. Though these compounds are highly active, they are poorly selective (**Table 1-3**). This could be because of change in conformation from a pyridinyl ring (planar) to piperidinyll ring (boat). This shed lights on the importance of planar conformation to selectively inhibit NOPR. Our SAR studies found that hydrophobic substitution with planar conformation (pyridine) attached to the carbon atom of the tropane ring is necessary for potent activity with selectivity.

We then compared the binding mode of compound 10 with SCH-221510 to identify the reasons for its potent activity than that of compound 10. Though both these compounds are highly similar, they differ in substitution in the tropane ring and the Cl atom at the phenyl rings has been replaced by methyl substitution respectively (**Supplementary Fig. S9**). The presence of hydroxyl (OH) at the tropane ring seems to be crucial as it may form a hydrogen bonding interaction with crucial Gln280 of NOPR. The hydrophobic methyl substitution at the phenyl ring of SCH-221510 might produce hydrophobic interactions with NOPR as there is a plenty of room at the respective position. These could be the possible reasons for potent activity than that of its derivative compound 10.

## Discussion

The NOPR was identified and sequenced from the human and mouse genome in 1994 as an orphan GPCR and considered an important drug target. We have been working on GPCR's using *in silico* methodologies<sup>34-36</sup> and we moved our focus on NOPR. Previously there were

reports on homology modeling of NOPR.<sup>31,32</sup> More recently there were reports on the homology modeling of active state NOPR and further molecular dynamics simulation studies for a short period.<sup>33</sup> However, no study has been previously conducted on the time dependent interactions between NOPR and agonists for long time using MDS. This paucity of data prompted us to undertake the present study to determine the effects of active site residues in the vicinity of ligand. With the availability of recently reported NOPR structure<sup>11</sup> we performed our study. The objective of this study was to analyze the behavior of NOPR-agonist complexes in a membrane environment and to characterize the reasons for activity.

As NOPR structure (**PDB code: 4EA3**) has already been reported, docking and molecular dynamic simulation studies were performed to better understand the binding mode between different agonists and NOPR. Moreover, it also helps us to elucidate the role of ligand molecules on the structure of transmembrane domain. We docked the natural agonist NOP, a small molecule agonist SCH-221510<sup>12</sup> and its derivative (compound 10)<sup>13</sup> into the active site of the receptor. The selection of binding mode was done based on interaction with crucial residues and scoring function. However results obtained from the docking study are far from conclusive since binding of an inhibitor to a receptor is a dynamic process. To gain further insights into the role of ligand molecules and its interaction with the receptor structure, molecular dynamics simulation was performed for 100 ns in the presence of membrane environment to better understand the SAR relations between NOPR and SCH-221510 derivatives.

As there are limitations arising from the small amount conformational sampling, we have performed a long run of 100 ns MDS for both complexes (NOPR-NOP peptide; NOPR-compound 10). The MDS analysis performed in the present study provides crucial insights of the binding site of NOPR. Our overall MDS studies of NOPR-agonist complexes found that Gln107,

Asp130, Tyr131, Met134, Ile219, Gln280 and Tyr309 are crucial which studies are in line with previous mutagenesis.<sup>13</sup> In addition, we found that residues such as Val126, Ile127, Ser223 (NOP peptide) and Trp276 are crucial and we believe that this warrants further mutagenesis studies. Our SAR studies showed that interaction between SCH-221510 derivatives and Asp130 is highly desirable. Hydrophobic substitution attached to the carbon atom of the tropane ring is also necessary. This stressed the importance of basic nitrogen and the hydrophobic substitution for potent activity. We then compared the binding mode of compound 10 with SCH-221510. The presence of hydroxyl (OH) at the tropane ring seems to be crucial as it may form a hydrogen bonding interaction with crucial Gln280 of NOPR. The hydrophobic methyl substitution at the phenyl ring of SCH-221510 might produce hydrophobic interactions with NOPR as there is a plenty of room at the respective position. These could be the possible reasons for potent activity than that of its derivative compound 10.

## Conclusion

NOPR is an important drug target for various diseases. In the present study, the time-dependent behavior of NOPR-agonist complexes was studied by molecular dynamics simulation. *In silico* methodologies, such as, docking, and molecular dynamics simulation studies (100 ns) were performed in an explicit lipid layer environment. Docking of NOP peptide and SCH-221510 and its derivative (compound 10) was done into the proposed binding site was performed. MDS was then performed with the docked structure for 100 ns. MDS showed the importance of the real time dynamic analysis. Relations between the properties of potent antagonists and binding site residues were sought and the possible binding orientations of agonists were deduced. The results of the present study may be valuable for further studies on site-directed mutagenesis or structure-based drug design targeting NOPR.

## References

- [1] C. Mollereau, M. Parmentier, P. Mailleux, J.L. Butour, C. Moisand, P. Chalon, D. Caput, G. Vassart, J.C. Meunier, ORL1, a novel member of the opioid receptor family: Cloning, functional expression and localization, *FEBS. Lett.*, 1994, 341, 33–38.
- [2] B.M. Cox, C. Chavkin, M.J. Christie, O. Civelli, C. Evans, M.D. Hamon, V. Hoellt, B. Kieffer, I. Kitchen, A.T. McKnight, J.C. Meunier, P.S. Portoghese, Opioid receptors. In: Girdlestone D, editor. *The IUPHAR compendium of receptor characterization and classification*, London: IUPHAR Media Ltd., 2000, 321–333.
- [3] J.C. Meunier, C. Mollereau, L. Toll, C. Suaudeau, C. Moisand, P. Alvinerie, J.L. Butour, J.C. Guillemot, P. Ferrara, B. Monsarrat, H. Mazarguil, G. Vassart, M. Parmentier, J. Costentin, Isolation and structure of the endogenous agonist of opioid receptor-like ORL1 receptor, *Nature.*, 1995, 377, 532–535.
- [4] R.K. Reinscheid, H.P. Nothacker, A. Bourson, A. Ardati, R.A. Henningsen, J.R. Bunzow, D.K. Grandy, H. Langen, F.R. Monsma Jr, O. Civelli, Orphanin FQ: A neuropeptide that activates an opioid-like G-protein coupled receptor, *Science.*, 1995, 270, 792–794.
- [5] N. Zaveri, W.E. Polgar, C.M. Olsen, A.B. Kelson, P. Grundt, J.W. Lewis, L. Toll, Characterization of opiates, neuroleptics, and synthetic analogs at ORL1 and opioid receptors, *Eur. J. Pharmacol.*, 2001, 428, 29–36.
- [6] D.G. Lambert, The nociceptin/orphanin FQ receptor: a target with broad therapeutic potential, *Nat. Rev. Drug Discov.*, 2008, 7, 694-710.

- [7] L.C. Chiou, Y.Y. Liao, P.C. Fan, P.H. Kuo, C.H. Wang, C. Riemer, E.P. Prinssen, Nociceptin/orphanin FQ receptors: pharmacology and clinical implications, *Curr. Drug Targets.*, 2007, 8, 117-135.
- [8] G.C. Bignan, P.J. Connoly, S.A. Middleton, Recent advances towards the discovery of ORL-1 receptor agonists and antagonists, *Expert. Opin. Ther. Pat.*, 2005, 5, 357–388.
- [9] M. Lazzeri, G. Calo, M. Spinelli, S. Malaguti, R. Guerrini, S. Salvadori, P. Beneforti, D. Regoli, D. Turini, Daily intravesical instillation of 1mg nociceptin/orphanin FQ for the control of neurogenic detrusor overactivity: A multicenter, placebo controlled, randomized exploratory study, *J. Urol.*, 2006, 176, 2098-2102.
- [10] L.W. Tari, The Utility of Structural Biology in Drug Discovery, Structure-Based Drug Discovery, *Methods in Molecular Biology.*, 2012, 841, 1-27.
- [11] A.A. Thompson, W. Liu, E. Chun, V. Katritch, H. Wu, E. Vardy, X.P. Huang, C. Trapella, R. Guerrini, G. Calo, B.L. Roth, V. Cherezov, R.C. Stevens, Structure of the nociceptin/orphanin FQ receptor in complex with a peptide mimetic, *Nature.*, 2012, 485, 395-399.
- [12] G.B. Varty, S.X. Lu, C.A. Morgan, M.E. Cohen-Williams, R.A. Hodgson, A. Smith-Torhan, H. Zhang, A.B. Fawzi, M.P. Graziano, G.D. Ho, J. Matasi, D. Tulshian, V.L. Coffin, G.J. Carey, The anxiolytic-like effects of the novel, orally active nociceptin opioid receptor agonist 8-[bis(2-methylphenyl)methyl]- 3-phenyl-8-azabicyclo[3.2.1]octan-3-ol (SCH 221510), *J. Pharmacol. Exp. Ther.* 2008, 326, 672–682.

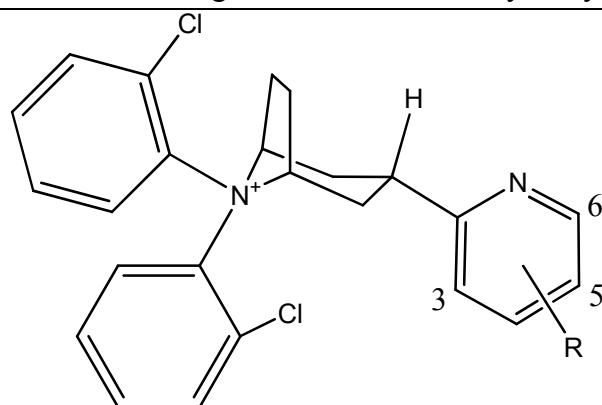
- [13] S.W. Yang, G. Ho, D. Tulshian, W.J. Greenlee, J. Anthes, X. Fernandez, R.L. McLeod, J.A. Hey, X. Xu, Discovery of Orally Active 3-Pyridinyl-tropane As a Potent Nociceptin Receptor Agonist for the Management of Cough, *J. Med. Chem.*, 2009, 52, 5323–5329.
- [14] M.J. Orsini, I. Nesmelova, H.C. Young, B. Hargittai, M.P. Beavers, J. Liu, P.J. Connolly, S.A. Middleton, K.H. Mayo, The nociceptin pharmacophore site for opioid receptor binding derived from the NMR structure and bioactivity relationships, *J. Biol. Chem.*, 2005, 280, 8134–8142.
- [15] SYBYL 8.1, Tripos International, 1699 South Hanley Rd., St. Louis, Missouri, 63144, USA.
- [16] G. Arfken, The method of steepest descents. n7.4. In: Holland B. and Singer T., editors. *Mathematical Methods for Physicists*, 3rd edn., Orlando, FL: Academic Press; 1985, p. 428–436.
- [16] D. van der Spoel, E. Lindahl, B. Hess, G. Groenhof, A.E. Mark, H.J. Berendsen H.J., GROMACS: fast, flexible and free, *J. Comput. Chem.*, 2005, 26, 1701–1718.
- [17] M. Clark M, R.D. Cramer, N. Vanopdenbosch, Validation of the general-purpose Tripos 5.2 force-field, *J. Comput. Chem.*, 1989, 10, 982–1012.
- [18] M.J.D. Powell, Restart procedures for the conjugate gradient method, *Math Program.*, 1977, 12, 241–254.
- [19] J. Gasteiger, M. Marsili, Iterative partial equalization of orbital electronegativity – a rapid access to atomic charges, *Tetrahedron.*, 1980, 36, 3219–3228.

- [20] R.D. Smith, J.B. Dunbar, P. M-U Ung, E.X. Esposito, C-Y Yang, CSAR Benchmark Exercise of 2010: Combined Evaluation Across All Submitted Scoring Functions, *J. Chem. Inf. Model.*, 2011, 51, 2115-2131.
- [21] D. Kozakov, D.R. Hall, D. Beglov, R. Brenke, S.R. Comeau, Y. Shen, K. Li, J. Zheng, P. Vakili, I.Ch. Paschalidis, S. Vajda, Achieving reliability and high accuracy in automated protein docking: ClusPro, PIPER, SDU, and stability analysis in CAPRI rounds 13–19, *Proteins.*, 2010, 78, 3124–3130.
- [22] C. Oostenbrink, A. Villa, A.E. Mark, W.F. Van Gunsteren, A biomolecular force field based on the free enthalpy of hydration and solvation: the GROMOS force-field parameter sets 53A5 and 53A6, *J. Comput. Chem.*, 2004, 25, 1656-1676.
- [23] D.P. Tieleman, J.L. MacCallum, W.L. Ash, C. Kandt, Z.T. Xu, L. Monticelli, Membrane protein simulations with a united-atom lipid and all-atom protein model: lipid–protein interactions, side chain transfer free energies and model proteins, *J. Phys. Condens. Matter.*, 2006, 18, S1221–S1234.
- [24] C. Kandt, W.L. Ash, D.P. Tieleman, Setting up and running molecular dynamics simulations of membrane proteins, *Methods.*, 2007, 41, 475-488.
- [25] W.L. Jorgensen, J. Chandrasekhar, J.D. Madura, R.W. Impey, M.L. Klein, Comparison of simple potential functions for simulating liquid water, *J. Chem. Phys.*, 1983, 79 926-935.
- [26] D.M.F. Aalten, R. Bywater, J.B.C. Findlay, M. Hendlich, R.W.W. Hooft, G. Vriend, PRODRG, a program for generating molecular topologies and unique molecular descriptors from coordinates of small molecules, *J. Comput. Aided Mol. Design.*, 1996, 10, 255-262.

- [27] J.A. Lemkul, W.J. Allen, D.R. Bevan, Practical Considerations for Building GROMOS-Compatible Small-Molecule Topologies, *J. Chem. Inf. Model.*, 2010, 50, 2221-2235.
- [28] T. Darden, D. York, L. Pedersen, Particle mesh ewald—an  $n \cdot \log(n)$  method for ewald sums in large systems, *J. Chem. Phys.*, 1993, 98, 10089–10092.
- [29] B. Hess, H. Bekker, H.J.C. Berendsen, J.G.E.M. Fraaije, LINCS: a linear constraint solver for molecular simulations, *J. Comput. Chem.*, 1997, 18, 1463-1472.
- [30] S. Miyamoto, P.A. Kollman, Settle, An analytical version of the SHAKE and RATTLE algorithm for rigid water molecules, *J. Comput. Chem.*, 1992, 13, 952-962.
- [31] C.M. Topham, L. Mouledous, G. Poda, B. Maigret, J.C. Meunier, Molecular modelling of the ORL1 receptor and its complex with nociceptin, *Protein. Eng.*, 1998, 11, 1163-1179.
- [32] N. Akuzawa, S. Takeda, M. Inshiguro, Structural modelling and mutation analysis of a nociceptin receptor and its ligand complexes, *J. Bio Chem.*, 2007, 141, 907-916.
- [33] P.R. Daga, N.T. Zaveri, Homology modeling and molecular dynamics simulations of the active state of the nociceptin receptor reveal new insights into agonist binding and activation, *Proteins.*, 2012, 80, 1948-1961.
- [34] G. Kothandan, C.G. Gadhe, T. Madhavan, S.J. Cho, Binding Site Analysis of CCR2 Through In Silico Methodologies: Docking, CoMFA, and CoMSIA, *Chem. Biol. Drug Des.*, 2011, 78, 161-174.
- [35] G. Kothandan, C.G. Gadhe, S.J. Cho, Structural insights from binding poses of CCR2 and CCR5 with clinically important antagonists: a combined in silico study, *Plos One.*, 2012, 7, e32864.

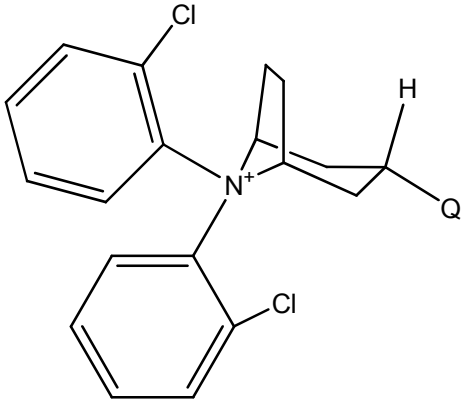
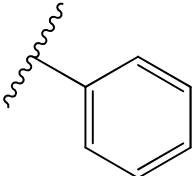
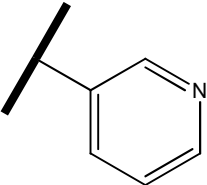
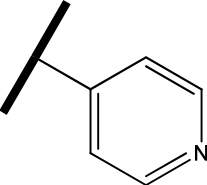
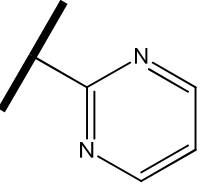
- [36] C.G. Gadhe, S.H. Lee, T. Madhavan, G. Kothandan, D. Choi, S.J. Cho, Ligand Based CoMFA, CoMSIA and HQSAR Analysis of CCR5 Antagonists, Bull. Korean Chem. Soc., 2010, 31, 2761-2770.

## Tables

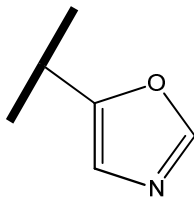
**Table 1** Structure and biological values of C-3 2-Pyridinyl derivatives

Compound	R	NOPR $K_i$ (nM)
10	H	5
18	5-F	34
19	5-Br	22
20	5-Me	14
21	5-OH	24
22	5-SMe	23
23	3-Me	29
24	3-Br	467
9	3-piperidinylmethyl	7
25	4-Me	18
26	6-F	25
27	6-Me	10
28	6-OMe	9

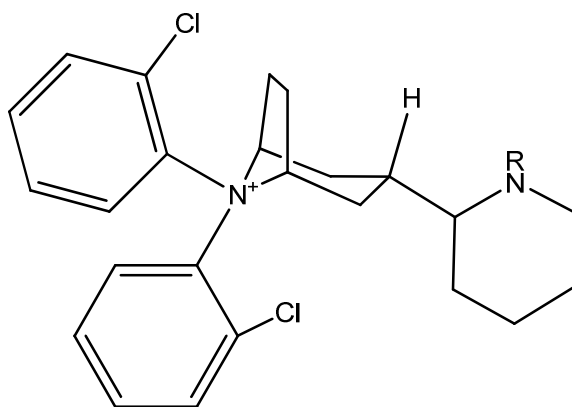
**Table 2** Structure and biological values of Additional C-3 Heterocyclic derivatives

Compound	Q	NOPR $K_i$ (nM)
		
29		9
30		5
31		69
32		6

17



272

**Table 3** Structure and biological values of C-3 2-Piperidinyl derivatives

Compound	R	NOPR $K_i$ (nM)
11	H	2
12	Me	1
13	Ac	71
14	-CH <sub>2</sub> CN	3
15	-(CH <sub>2</sub> ) <sub>2</sub> OH	2

## Figure Legends

**Fig. 1** Structures of NOP peptide and NOPR. (a) Modeled and energy minimized structure of NOP peptide. (b) Energy minimized structure of NOPR. The helix regions are shown in red, whereas the sheets and loops are colored in green and yellow.

**Fig. 2** Binding mode of agonist SCH-221510 inside the binding site. Hydrogen bonding is colored in red. Binding site residues are colored based on atom types. Fig. generated using the Pymol program (<http://www.pymol.org>).

**Fig. 3** Binding mode of agonist compound 10 inside the binding site. Hydrogen bonding is colored in red. Binding site residues are colored based on atom types. Fig. generated using the Pymol program (<http://www.pymol.org>).

**Fig. 4** Binding mode of agonist NOP peptide inside the binding site. Hydrogen bonding is colored in red. . Receptor structure is shown in surfaces and the peptide structure is shown in cartoon. Binding site residues are colored based on atom types. Receptor residues are labeled in triple letter code and the peptide residues are labeled in single letter code. Fig. generated using the Pymol program (<http://www.pymol.org>).

**Fig. 5** Side view of NOPR-agonist-membrane-aqueous environment for a production runs of 100 ns MDS. (a) Setup of NOPR-compound 10-lipids-water molecules. Seven transmembrane helices are represented as cartoons, the ligand molecule as a surface, lipid molecules as lines, and water molecules as sticks (b) Setup of NOPR-NOP peptide-lipids-water molecules. Seven transmembrane helices are represented as cartoons, the ligand molecule as a cartoon (red), lipid molecules as lines, and water molecules as sticks Fig. generated using the Pymol program (<http://www.pymol.org>).

**Fig. 6** Structural analysis of NOPR-NOP peptide complex throughout production run (a) Total energy plot of the MD simulation and variations in system total energy over 100 ns. (b) Root mean square deviation (RMSD) plot for NOPR (C $\alpha$  – Black) and NOP peptide (red) from initial structures throughout the 100 ns simulation as a function of time. Structural analysis of NOPR-compound 10 complex throughout production run (c) Total energy plot of the MD simulation and variations in system total energy over 100 ns. (d) Root mean square deviation (RMSD) plot for NOPR (C $\alpha$  – Black) and compound 10 (red) from initial structures throughout the 100 ns simulation as a function of time.

**Fig. 7** Importance of Asp130 throughout the production run (a) Minimum distance between Asp130 and nitrogen atom of the tropane ring of ligand over 100 ns. (b) Hydrogen bonding between Asp130 and protonated nitrogen of the ligand throughout the 100 ns simulation as a function of time.

**Fig. 8** Importance of Tyr131, Tyr132, Met134 and Phe135 throughout the production run. (a) Minimum distance between Tyr131 (black), Tyr132 (red) and the ligand molecule. (b) Minimum distance between Met134 (black), Phe135 (red) and the ligand molecule. Fig. generated using xmgrace plotting software.

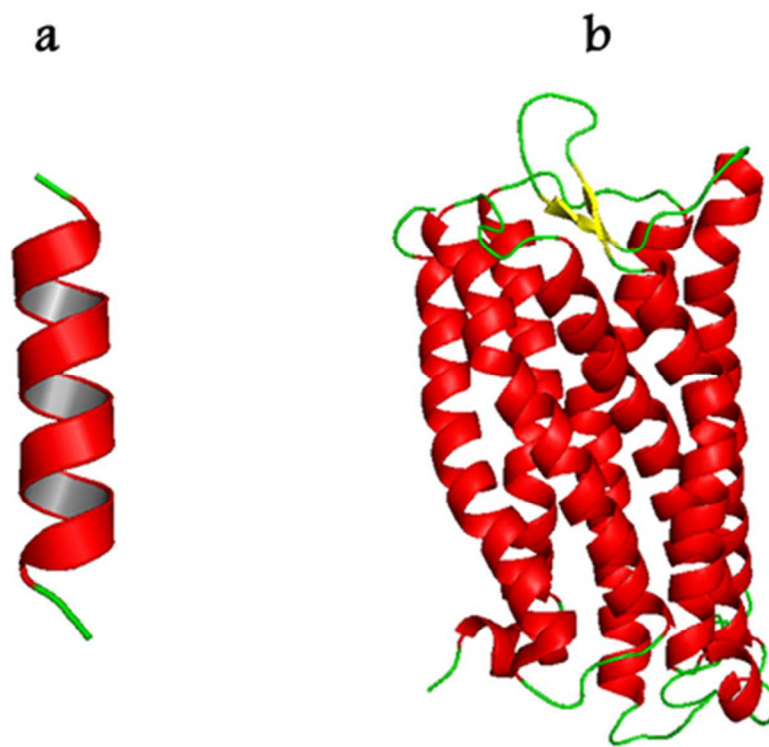


Fig. 1 Structures of NOP peptide and NOPR. (a) Modeled and energy minimized structure of NOP peptide. (b) Energy minimized structure of NOPR. The helix regions are shown in red, whereas the sheets and loops are colored in green and yellow.  
33x32mm (300 x 300 DPI)

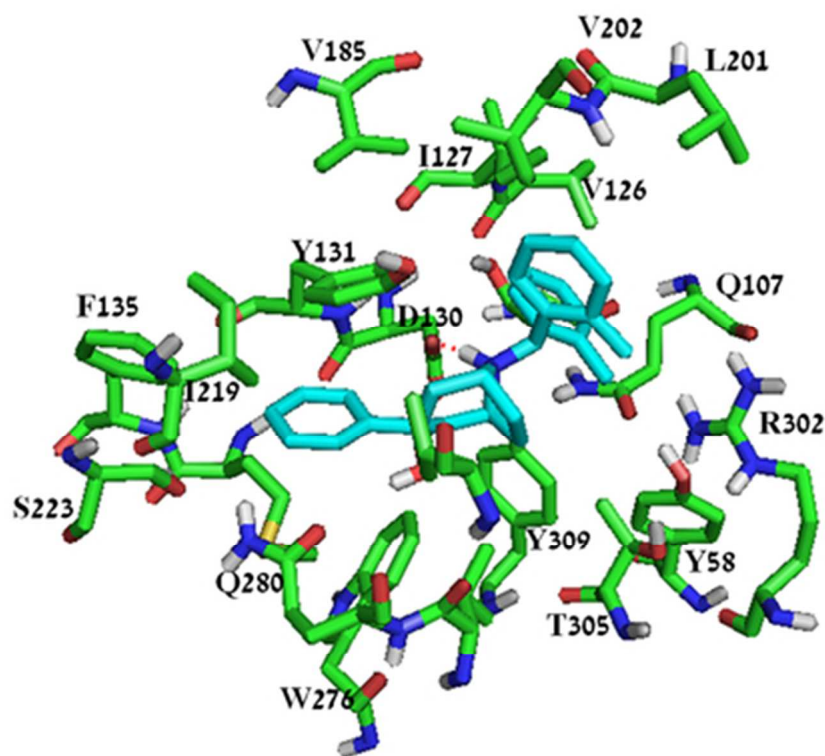


Fig. 2 Binding mode of agonist SCH-221510 inside the binding site. Hydrogen bonding is colored in red. Binding site residues are colored based on atom types. Fig. generated using the Pymol program (<http://www.pymol.org>). 35x32mm (300 x 300 DPI)

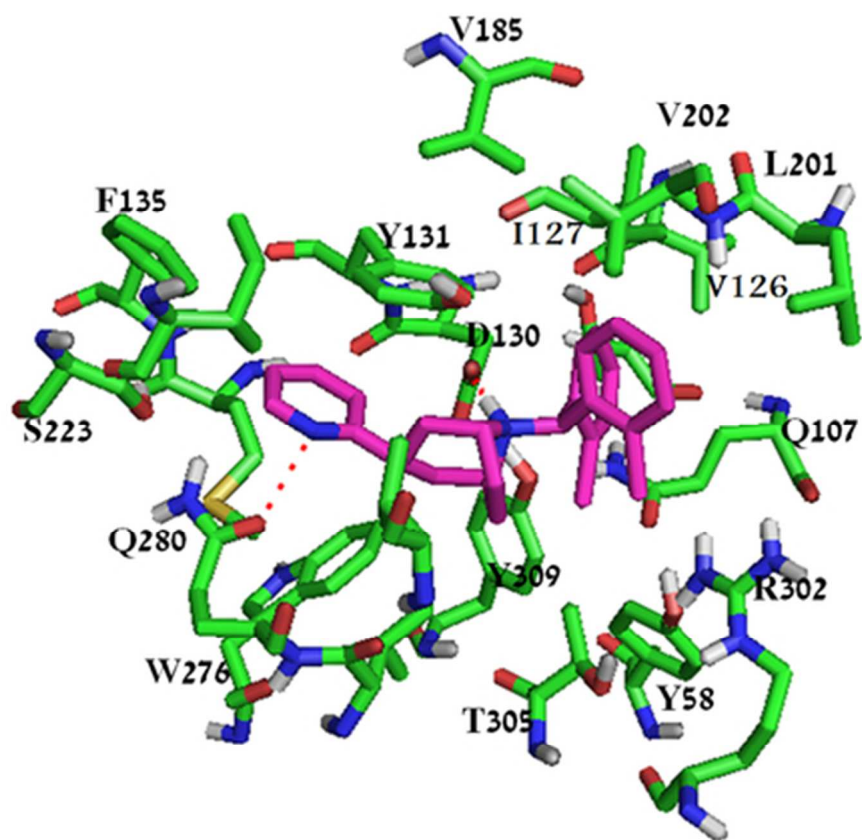


Fig. 3 Binding mode of agonist compound 10 inside the binding site. Hydrogen bonding is colored in red. Binding site residues are colored based on atom types. Fig. generated using the Pymol program (<http://www.pymol.org>). 37x36mm (300 x 300 DPI)

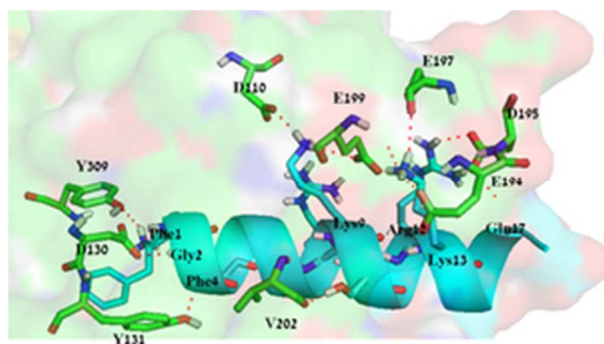


Fig. 4 Binding mode of agonist NOP peptide inside the binding site. Hydrogen bonding is colored in red. . Receptor structure is shown in surfaces and the peptide structure is shown in cartoon. Binding site residues are colored based on atom types. Receptor residues are labeled in triple letter code and the peptide residues are labeled in single letter code. Fig. generated using the Pymol program (<http://www.pymol.org>).  
25x14mm (300 x 300 DPI)

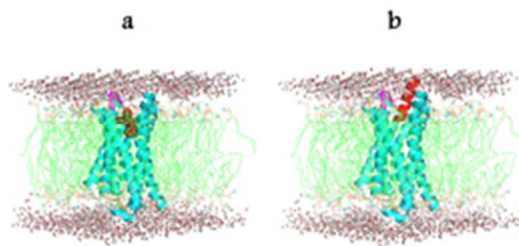


Fig. 5 Side view of NOPR-agonist-membrane-aqueous environment for a production runs of 100 ns MDS. (a) Setup of NOPR-compound 10-lipids-water molecules. Seven transmembrane helices are represented as cartoons, the ligand molecule as a surface, lipid molecules as lines, and water molecules as sticks (b) Setup of NOPR-NOP peptide-lipids-water molecules. Seven transmembrane helices are represented as cartoons, the ligand molecule as a cartoon (red), lipid molecules as lines, and water molecules as sticks Fig. generated using the Pymol program (<http://www.pymol.org>).  
21x10mm (300 x 300 DPI)

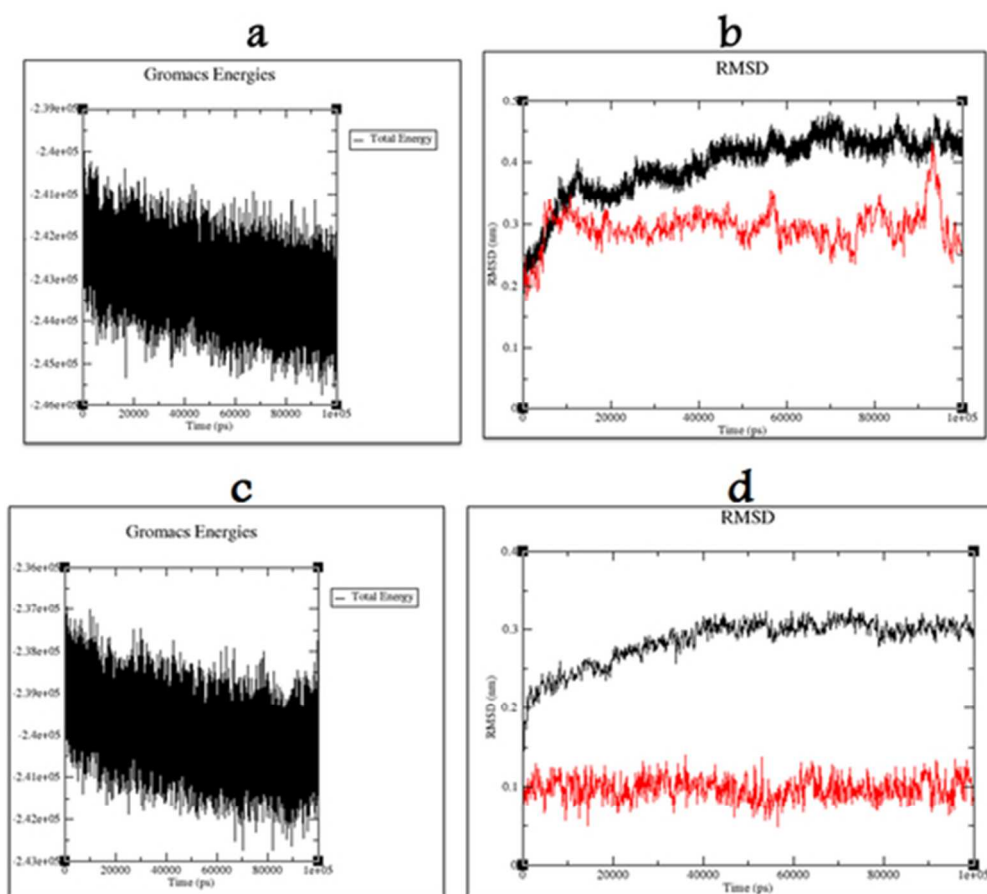


Fig. 6 Structural analysis of NOPR-NOP peptide complex throughout production run (a) Total energy plot of the MD simulation and variations in system total energy over 100 ns. (b) Root mean square deviation (RMSD) plot for NOPR (Ca - Black) and NOP peptide (red) from initial structures throughout the 100 ns simulation as a function of time. Structural analysis of NOPR-compound 10 complex throughout production run (c) Total energy plot of the MD simulation and variations in system total energy over 100 ns. (d) Root mean square deviation (RMSD) plot for NOPR (Ca - Black) and compound 10 (red) from initial structures throughout the 100 ns simulation as a function of time.

43x39mm (300 x 300 DPI)

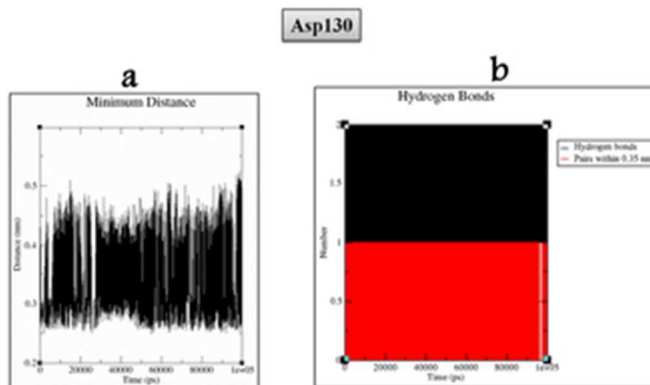


Fig. 7 Importance of Asp130 throughout the production run (a) Minimum distance between Asp130 and nitrogen atom of the tropane ring of ligand over 100 ns. (b) Hydrogen bonding between Asp130 and protonated nitrogen of the ligand throughout the 100 ns simulation as a function of time.  
27x16mm (300 x 300 DPI)

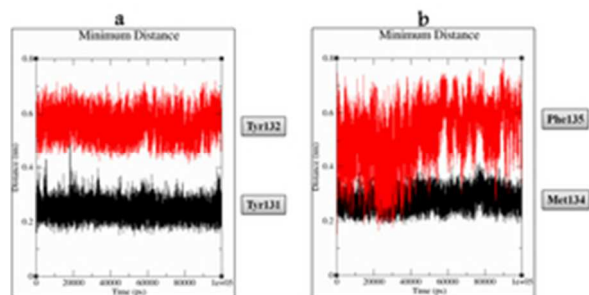


Fig. 8 Importance of Tyr131, Tyr132, Met134 and Phe135 throughout the production run. (a) Minimum distance between Tyr131 (black), Tyr132 (red) and the ligand molecule. (b) Minimum distance between Met134 (black), Phe135 (red) and the ligand molecule. Fig. generated using xmgrace plotting software. 24x12mm (300 x 300 DPI)